Characterization of Cavitation Instabilities in Axial Inducers by Means of High-Speed Movies

Angelo Cervone[*], Lucio Torre[†], Domenico Fotino[‡], Luca d'Agostino[§]
ALTA S.p.A. - Via Gherardesca, 5 - 56121 Ospedaletto, Pisa, Italy

and

Cristina Bramanti [∞]
ESA-ESTEC, Keplerlaan 1, Nordwijk, The Netherlands

The present paper illustrates the set-up and the preliminary results of an experimental investigation of cavitation flow instabilities carried out by means of a high-speed camera on a three bladed inducer in the CPRTF (Cavitating Pump Rotordynamic Test Facility) at Alta S.p.A. The brightness thresholding technique adopted for cavitation recognition is described. A semi-automatic binary algorithm has been used for processing high speed videos of the cavitating inducer. In order to test the capabilities of the algorithm, the mean frontal cavitating area has been computed under different operating conditions. The tip cavity length has also been evaluated as a function of time. Fourier analysis showed the occurrence of a cavity length oscillation at a frequency of 15.7 Hz, which corresponds to the frequency of the rotating stall instability previously detected on the same inducer by means of pressure oscillations analysis.

Nomenclature

A	=	amplitude of oscillations
f	=	frequency
p_{in}	=	inlet pressure
p_V	=	vapor pressure
Q	=	volumetric flow rate
r_T	=	inducer blade tip radius
S_{cav}	=	total cavitating surface on each blade
S_{flow}	=	inducer frontal surface
Ω	=	rotational speed
Φ	=	flow coefficient $\Phi = \dfrac{Q}{\pi \Omega r_T^3}$
ϕ	=	phase of oscillations
ρ	=	density
σ	=	cavitation number
$\Delta\theta$	=	azimuthal extension of the cavity at the tip of the blades

[*] Project manager, ALTA S.p.A., AIAA Member; a.cervone@alta-space.com
[†] Project engineer, ALTA S.p.A., AIAA Member; l.torre@alta-space.com
[‡] MS student, Department of Aerospace Engineering – University of Pisa; domenico.fotino@tiscalinet.it
[∞] Post-Doc Fellow, ESA Advanced Concepts Team, AIAA member; Cristina.Bramanti@esa.int
[§] Professor, Department of Aerospace Engineering – University of Pisa, AIAA Member; luca.dagostino@ing.unipi.it

I. Introduction

In space propulsion, propellant feed turbopumps are a crucial component of all primary propulsion concepts powered by liquid propellant rocket engines. Severe limitations are associated with the design of high power density, dynamically stable machines capable of meeting the extremely demanding suction, pumping and reliability requirements of current space transportation systems (Stripling & Acosta[1], 1962).

In time, the quest for weight reduction has led to the design of faster and lighter turbopumps. For this reason, current rocket propellant feed turbopumps are often operated at supercritical conditions, where rotordynamic instabilities and cavitation become especially important. Axial inducers are typically used in order to avoid unacceptable cavitation in the centrifugal stage of the pump. Inducers normally operate under cavitating conditions which can cause blade erosion, decrease of the head performance and the onset of dangerous fluid dynamic or rotordynamic instabilities.

According to Brennen[2] (1994), these flow instabilities can be divided in three main categories: global oscillations, local oscillations and instabilities caused by radial or rotordynamic forces. Some of the most interesting and well-recognized instabilities in pumps and axial inducers are global oscillations, such as the *rotating stall* and the *rotating cavitation*, propagating in the azimuthal direction at angular speeds different from that of the pump (typically subsynchronous for rotating stall and supersynchronous for rotating cavitation), Other global oscillations are the *surge* and the *cavitation auto-oscillations*, system instabilities involving strong longitudinal flow and pressure oscillations of the whole suction line, typically occurring in noncavitating pumps for positive slopes of the characteristic curve (surge) and near breakdown conditions in cavitating turbopumps (cavitation auto-oscillations).

Experimental investigations on the instabilities triggered by cavitation in axial inducers have been recently carried out at Alta S.p.A. (Cervone, Testa, Bramanti, Rapposelli and d'Agostino[3], 2005; Cervone, Torre, Bramanti., Rapposelli and d'Agostino[4], 2005). Experiments were conducted in the CPTF (Cavitating Pump Test Facility), specifically intended for general-purpose experimentation on cavitating/noncavitating turbopumps, and its upgraded version, the CPRTF (Cavitating Pump Rotordynamic Test Facility), which is especially dedicated to the investigation of rotordynamic fluid forces in forced vibration experiments with adjustable rotational and whirl speeds.

The frequency of oscillation and the spatial characteristics (i.e. rotating or axial) of the detected instabilities can be analyzed by means of the cross-correlation and phase analysis technique introduced for the first time by Tsujimoto and his collaborators[5] in 1997. This technique has also been used in Alta's experiments[3,4].

In order to better understand the nature and the characteristics of the flow instabilities triggered by cavitation, high speed video movies can be used in combination with pressure oscillations measurements. The capability of recording movies at very high frame rates opens the possibility of analyzing the evolution of cavitation on the blades and, as a consequence, of classifying and better understand the characteristics of the detected instabilities. Using the combination of these techniques, Tsujimoto and his collaborators[5] detected the occurrence of rotating cavitation and other modes of oscillation on a scaled model of the LE-7 LOX turbopump inducer. They concluded that the rotating cavitation was probably caused by the occurrence of five cavitation regions extending upstream from the tip of the blades and slowly rotating. By analysis of the high-speed movies they also detected a form of instability characterized by axial fluctuations (cavitation surge).

Hashimoto *et al.*[6] used a high speed camera at 7000 fps to plot the cavitating surface, as a function of time, on a three bladed inducer with dimensions similar to those of the LE-7 LOX pump inducer. They detected various modes of oscillation, including a backward-rotating and a forward-rotating cavitation, an attached cavitation and a low cycle oscillation.

Other recent results obtained in Japanese research laboratories using high speed cameras (Kamijo *et al.*[7], 1994), confirmed the occurrence of a supersynchronous frequency due to circumferential cavity length oscillations. They observed that both the tip vortex cavitation and the blade surface cavitation oscillate at approximately the same supersynchronous frequency and the same phase.

This paper is aimed at illustrating the results of an experimental investigation carried out on a three bladed inducer by means of a high-speed camera, capable of recording video movies at a frame rate up to 16000 fps. The procedures and algorithms used to analyze the frames are widely described. High-speed movies of the cavitating inducer have been recorded at different flow conditions, chosen based on the results of the previous investigations on pressure fluctuations, in order to better highlight the correlation between the detected instabilities and the optical visualization of cavitation on the pump blades. Front and side movies of the pumps have been used for the investigation. Cross-correlation of different frame images has also been employed to analyze the characteristics and the development of the cavitating region on each blade during inducer rotation.

II. Experimental Apparatus

The Cavitating Pump Rotordynamic Test Facility (CPRTF, Figure 1) has been designed to experimentally characterize the performance of pumps in a wide variety of alternative configurations (axial, radial or mixed flow, with or without an inducer; Rapposelli, Cervone and d'Agostino[8], 2002). The facility operates in water at temperatures up to 90 °C and is intended as a flexible apparatus readily adaptable to conduct experimental investigations on virtually any kind of fluid dynamic phenomena relevant to high performance turbopumps. The test section (Figure 2) is equipped with a rotating dynamometer, for the measurement of the forces and moments acting on the impeller, and a mechanism for adjusting and rotating the eccentricity of the impeller axis in the range 0÷2 mm and ±3000 rpm. The inlet section, made of Plexiglas, is transparent in order to allow for optical visualization of cavitation on the test inducer.

The adjustable physical parameters of the experimental set-up include the pump rotating speed and acceleration (by means of the engine controls), the mass flow (by means of a lamination valve), the temperature and pressure of the working fluid (by means, respectively, of a heat exchanger and a bladder placed inside the tank).

For the present experimental work the facility was assembled in a simplified configuration without the rotating dynamometer. The test section was equipped with three different series of pressure transducers. The inlet pressure is measured by means of an absolute pressure transducer installed upstream of the Plexiglas inlet section (Druck, model PMP 1400, 0÷1.5 bar operating range, 0.25% precision class). The pressure rise, necessary for the characterization of the pump performance, is measured by means of two redundant differential pressure transducers installed between the inlet and the outlet sections of the test pump (Kulite, model BMD 1P 1500 100, 0-100 psid operating range, 0.1% precision class; Druck, model PMP 4170, 0÷1 bard operating range, 0.08% precision class). The pressure fluctuations are analyzed by equipping the inlet section (Figure 3) with flush-mounted piezoelectric pressure transducers (PCB M112A22, ICP® voltage mode-type, 0.1% class) located at three axial stations (inducer inlet, outlet and at the middle of the axial chord of the blades). At each axial station at least two transducers have to be mounted with a given angular spacing, in order to cross-correlate their signals for coherence and phase analysis. As a result, waterfall plots of the power spectral density of the pressure fluctuations can be obtained as functions of the cavitation number $\sigma = (p_{in} - p_V) / \frac{1}{2}\rho\Omega^2 r_T^2$, in order to detect the occurence of instabilities. The axial or azimuthal nature of the detected instabilities (and, in the second case, the number of rotating cells involved) can be determined by means of cross-correlation of the pressure signals from different locations.

The capabilities of the test facility have been improved after the installation of an integrated system for the optical analysis of the cavitating flow. The core of the system is represented by a high-speed video camera, Fastec Imaging model Ranger having a record rate variable from 125 fps (max resolution 1280x1024) to 16000 fps (max resolution

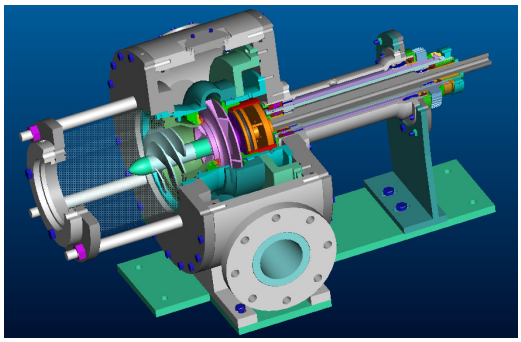

Figure 2. Cut-out drawing of the CPRTF test section.

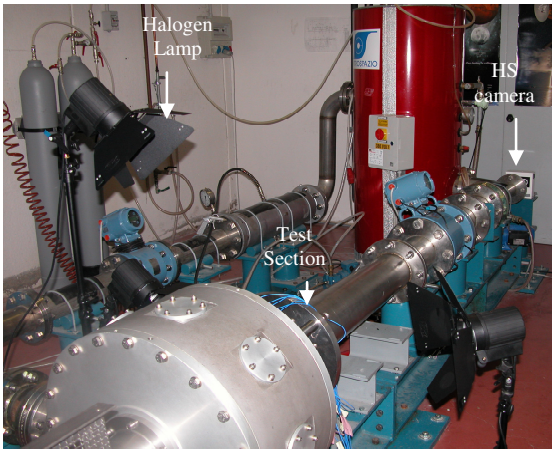

Figure 1. The Cavitating Pump Rotordynamic Test Facility.

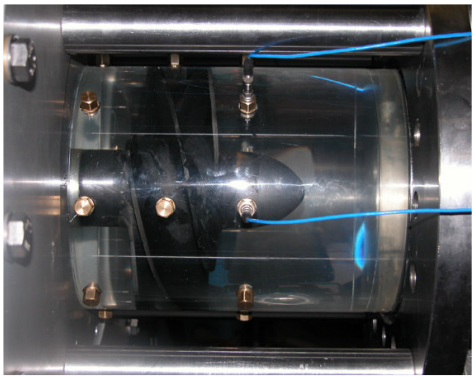

Figure 3. The inlet section of the facility instrumented with piezoelectric pressure transducers.

1280x32). It uses a monochrome CMOS sensor and its recording mode can be manual or triggered by the connection with a Personal Computer by means of USB port. The shutter speed ranges from 1x to 20x the recording rate. The required illumination level is provided by three halogen lamps produced by Hedler, each one having a power of 1250 W. The camera can also be synchronized with a stroboscopic light, Drelloscop 3009, having a maximum flash frequency of 1000 lamps/second with a frequency accuracy of 0.001%. The optical system is completed by a Nikon Coolpix 5700 digital photo camera, with optical 8x zoom, digital 4x zoom, a focal distance from 8.9 to 71.2 millimeters and a shutter speed from 1/4000 sec to 8 sec.

The characteristics of the facility make it possible to record both side movies, through the Plexiglas inlet section, and frontal movies, through an optical access placed at the end of the suction line (Figure 1). Side movies provide indications on the extension of cavitation in the blade channels, whereas the frontal ones give information about the radial and circumferential extension of the cavities on the blades.

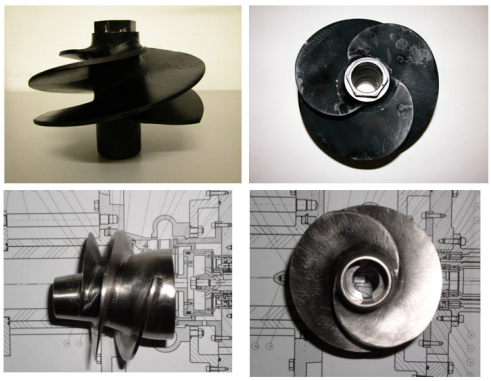

Figure 4. The FIP162 inducer (top) and the FAST2 inducer (bottom).

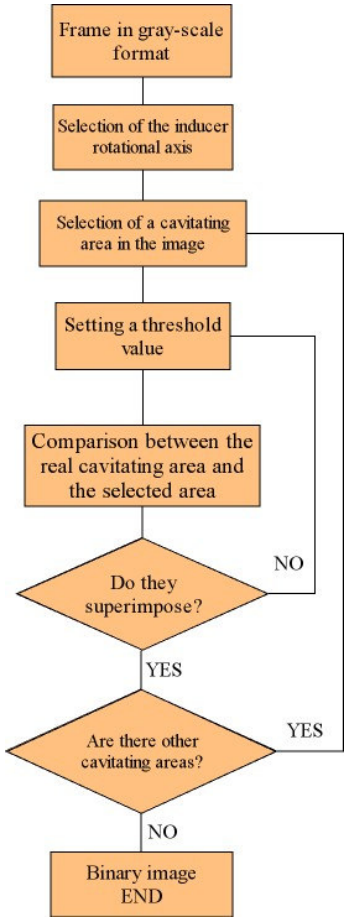

Figure 5. Flow chart of the image processing algorithm.

III. Test Inducers

The images and preliminary results showed in this paper refer to two axial pumps, the FIP162 inducer and the FAST2 inducer (Figure 4). The FIP162 is a 3-bladed, aluminum-made inducer of extremely simple helical geometry, with a tip radius of 81 mm, a hub radius of 22.5 mm, a tip blade angle of 9°, a tip solidity of 3.05 and 2 mm thick back-swept blades with blunt leading and trailing edges. It is manufactured by Fabbrica Italiana Pompe (FIP) S.p.A. for the food industry by welding the blades on the hub, and therefore it does not satisfy stringent geometric tolerances. The FAST2 inducer, on the other side, is a two-bladed stainless steel axial inducer with a tip radius of 41.1 mm and a profiled, variable-radius hub (15 mm inlet radius, 28 mm outlet radius). The blades are backswept, with variable thickness and nonuniform blade angle. The inlet tip blade angle is 7.38°, the outlet tip blade angle is 21.24° and the tip solidity is 1.59. This inducer has been designed by Avio S.p.A. using the criteria followed for VINCI180 inducer and taking into account the results derived from past experience (VULCAIN MK1 and MK2, ATE, VINCI150).

IV. Image Processing Algorithm

An image processing algorithm has been developed to characterize the regions of the image where cavitation is present. This algorithm has been implemented in a code that allows for automatically processing the frames of the movies taken by the high-speed camera and for analyzing the movie using the processed frames. The algorithm has been implemented in *Matlab*® and its flow chart is shown in Figure 5. The input is a frame in gray-scale format: a typical input frontal image is shown in Figure 6 (a) whereas a typical input side image is shown in Figure 7 (left).

It is important to identify the position of the inducer rotational axis with good precision in every frame, in order to rotate all the processed frames around this point and obtain a movie in which the position of the blades is fixed. It is therefore possible to

characterize the development of the cavitating surface on the blades in order to detect possible oscillations. The rotational axis is manually selected on the image, while the angle of rotation of every frame around this point can be simply calculated as a function of the inducer rotational speed and the sample rate at which the movie has been taken.

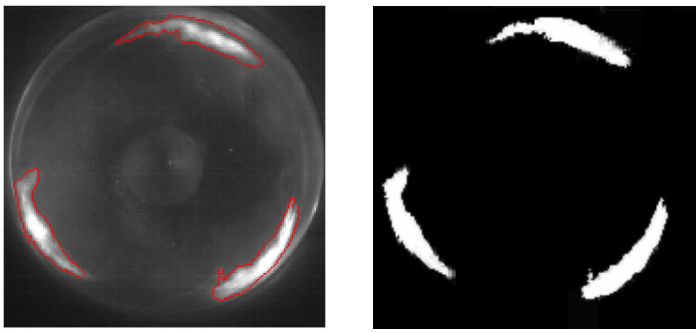

(a) **(b)**

Figure 6. Comparison between the original frame (a) and the processed binary image (b) in a sample case.

The next step of the algorithm is the so-called "segmentation technique", by which the cavitating regions are separated by the rest of the image. Several segmentation techniques have been proposed in the past by the open literature (see for example Gonzales[9]), but the most widely used are the edge detection algorithms and the thresholding technique (see respectively Hiscock *et al.*[10], Kato *et al.*[11]). In the present paper, the thresholding technique has been used. By this technique, the original grayscale image is converted in a binary image: the pixels having an intensity in the original image greater than a certain threshold value are set equal to 1 (i.e., they become white pixels), while all other pixels are set equal to 0 (i.e., they become black pixels). Despite its implementation simplicity, the main problem of this technique is the evaluation of the right value to be attributed to the threshold. There are several methods to automatically find this value according to the image histogram properties (Gonzalez[9], Kato *et al.*[11], Otsu[12]). Typical luminosity histograms of the cavitating areas show double peaks and a good choice for the threshold value is represented by the value between the peaks (Figure 7).

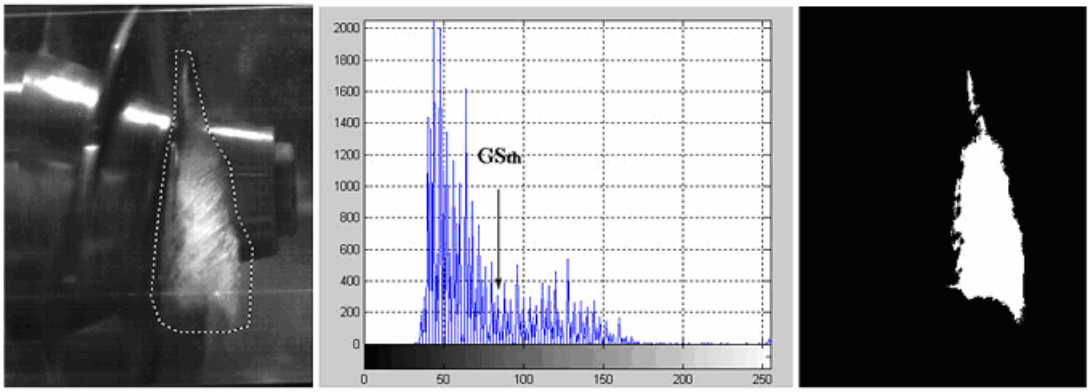

Figure 7. Selection of the cavitating area on a grayscale image (left), luminosity histogram (center) and binarized image (right). Inducer: FAST2, Flow conditions: Φ = 0.040, σ = 0.16, Ω = 3000 rpm.

Sometimes the histogram does not show two clearly distinguished peaks and the threshold value can then be found by a trial-and-error technique until the right value is found (i.e. the value that produces a good result as by the operator's judgement [Gonzalez[9]]). In the present case it has not been possible to find a threshold value for the frame as a whole, so different threshold values have been used for the different cavitating regions in the image. These regions are manually selected (Figure 7) and the threshold value is given at the end of an iterative procedure whose first trial value is given automatically by the Otsu's method (Otsu[12]).

As an example, Figure 6(b) shows the results obtained applying the above algorithm to the frame shown in Figure 6(a). In the Figure, the edge of the detected cavitating regions is superimposed to the original frame (red contour).

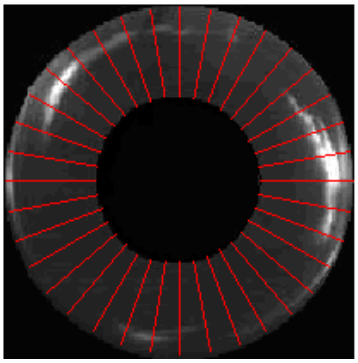

Figure 8. Example of the image division and the masked portions.

In order to improve the computational time, a semi-automatic algorithm has been developed (see the flow chart in Figure 9). The input

frame is divided in many circular sectors (Figure 8) and an automatic threshold value, evaluated using the Otsu's method, is given for each sector. By calibrating the angular division of the frame it is possible to obtain two well distinguished peaks in the histogram for each sector. This allows for obtaining a good first-tentative image segmentation. In order to better analyze the cavitating regions on the blades, the central portion of the image (where other cavitating phenomena often occur) and the region outside the inducer are covered with black pixels (masked portions in Figure 8). If the white regions in the first-tentative binarized image do not superimpose to the effective cavitating regions of the original frame, the operator can manually process the frame selecting the right cavitating areas and a new threshold value.

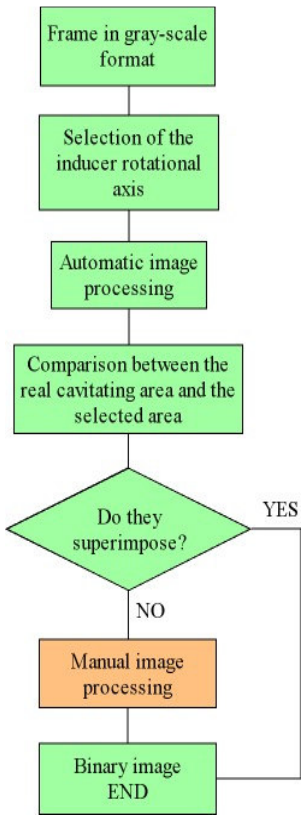

Figure 9. Flow chart of the semi-automatic algorithm.

V. Results and Discussion

A. Procedure

The working fluid has been deareated before every test. In order to improve the image quality, excessively high cavitation levels have not been reached during the tests. For this reason, the inducer rotational speed has been set equal to 1500 rpm. High speed movies have been recorded at constant flow rate, while the inducer inlet pressure has been decreased from high to low values using the vacuum pump.

The camera frame rate has been set equal to 1000 fps (i.e. 40 frames/revolution at 1500 rpm), at an image resolution of 640x480 pixels. This setup gave the possibility of optically analyzing the cavitation instabilities previously detected on the same inducer by unsteady pressure measurement analysis[3].

B. Analysis of the cavitating surface on the blades

The first plot, presented in Figure 10(a), shows the normalized frontal cavitating surface as a function of the flow coefficient for several cavitation numbers. The total frontal area of the cavitating regions on the inducer blades (S_{cav}) has been estimated by mediating the number of white pixels in all the frames of a movie taken at given flow conditions. This value has been normalized using the total frontal area of the inducer (S_{flow}).

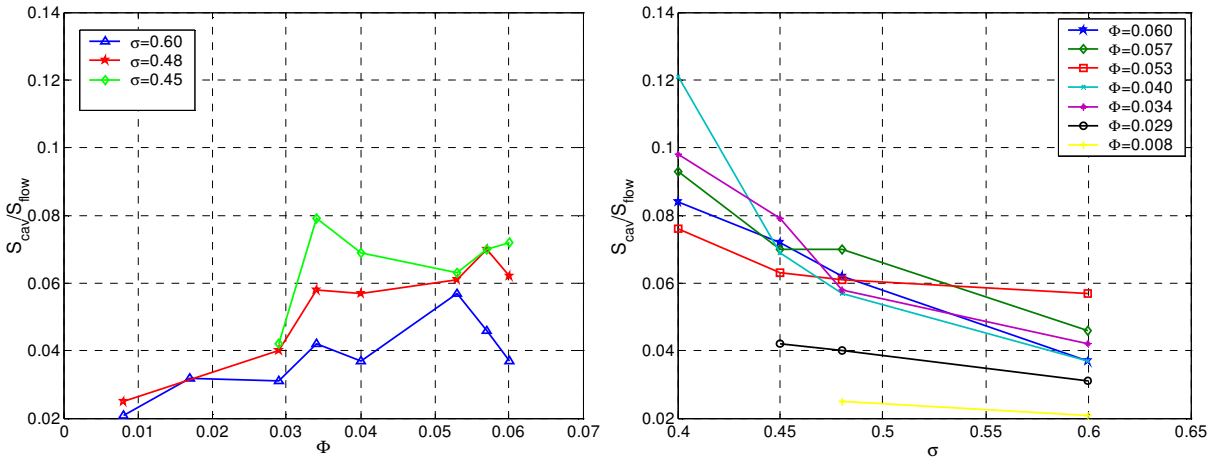

(a) **(b)**

Figure 10. Frontal cavitating surface (normalized with the frontal area of the inducer) as a function of the flow coefficient for several values of the cavitation number (a) and as a function of the cavitation number for several values of the flow coefficient (b). Inducer: FIP162, Ω=1500 rpm, frame sample rate = 1000 fps.

By examination of Figure 10(a) it can be observed that the cavitating surface tends to decrease when the flow coefficient decreases. At lower flow coefficients and cavitation numbers, the image processing algorithm described in the previous Section can not be used properly, due to the significant number of vortices and large cavitation regions in the inducer inlet flow. The water quality is significantly degraded, with a large number of cavitating nuclei and consequently adverse effects on light diffusion (Figure 11).

In the plot of Figure 10(a) it can also be observed that the cavitating surface tends to decrease when the cavitation number increases. This is better shown by Figure 10(b), where the normalized frontal area of the cavitating surface is shown as a function of the cavitation number for several flow coefficients. This aspect is evident by observation of the frames shown in Figure 12 and referred to a particular value of the flow coefficient.

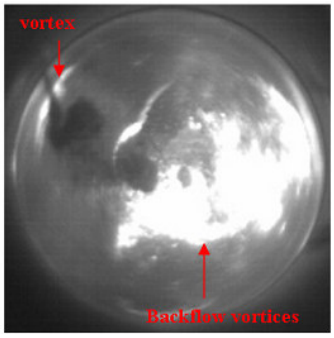

Figure 11. Example of a frame which can not be analyzed using the image processing algorithm.

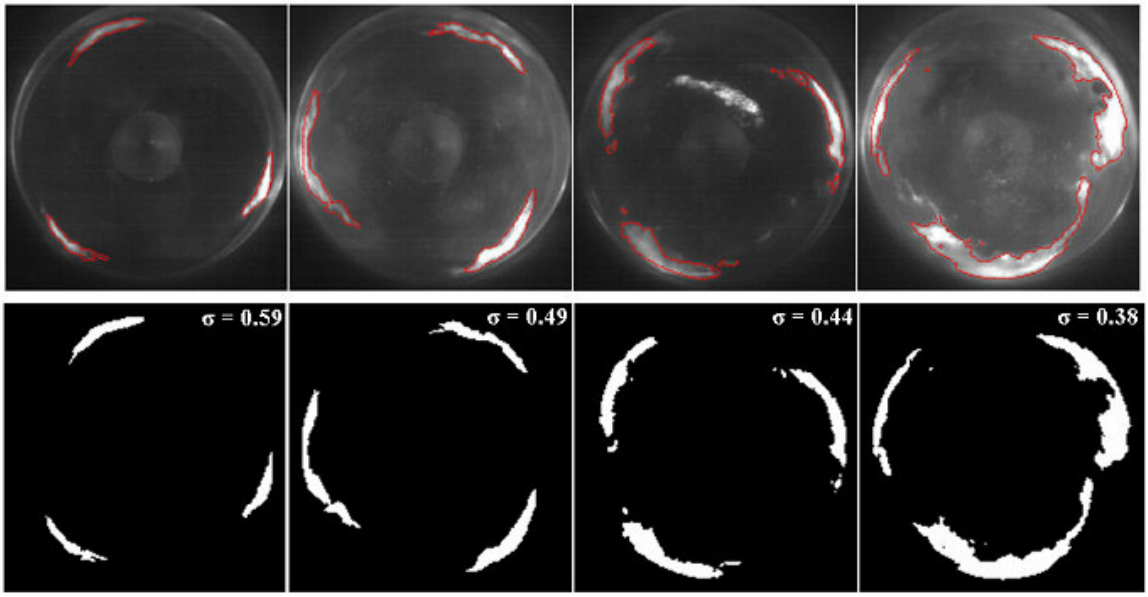

Figure 12. Original frames (top) and elaborated frames (bottom) for a particular flow condition. (Φ =0.04, Ω= 1500 rpm, frame sample rate = 1000 fps).

C. Tip cavity length estimation

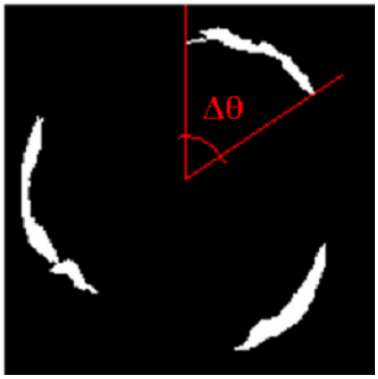

Figure 13. Evaluation of the azimuthal extension of the cavitation on a blade.

The tip cavity length has been estimated using an automatic algorithm which scans every binarized frame with a line rotating around the inducer axis with an angular pitch of 1°. When a white pixel is found along the scanning line after a completely black line, the cavitating region is assumed to begin; on the other hand, when every pixel along the scanning line becomes black, the cavitating region is assumed to finish (Figure 13). The length of the cavitating region is finally estimated by multiplying the azimuthal extension $\Delta\theta$ by the radius at which the cavitating region has been examined.

This procedure has been applied to a binarized movie whose frames have been rotated around the inducer rotational axis in order to obtain fixed blade position. The following plots (Figure 14) show the length of the cavitating region on the blades as a function of time, for given flow conditions.

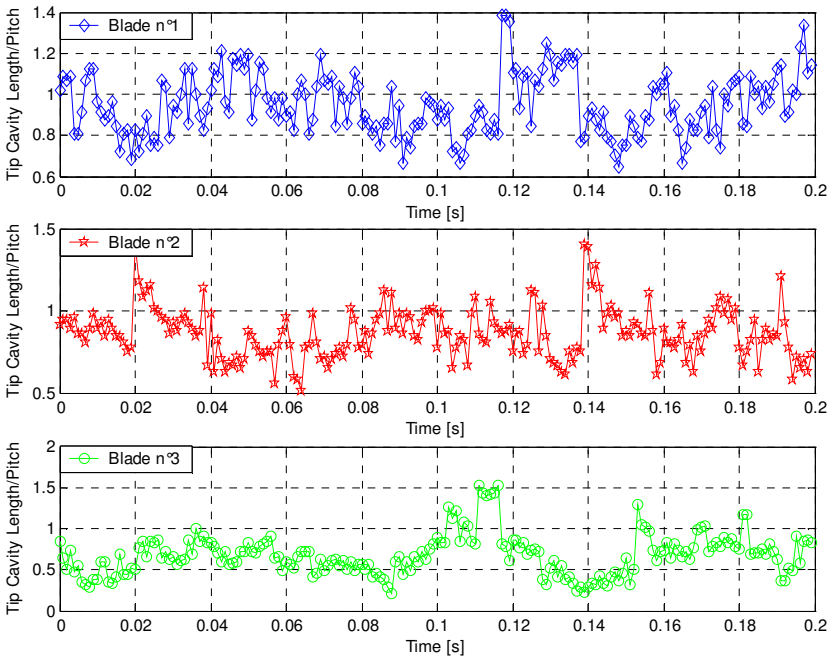

Figure 14. Length of the cavitating region on the blades as a function of time (Φ = 0.034, σ = 0.50, Ω = 1500 rpm, frame sample rate = 1000 fps).

Sometimes the cavitating region appears to be fragmented. This is due to the separation of small cavitating regions and to the presence of vortexes between the real blade surface and the camera lens (Figure 11). In this case the algorithm takes into account the angular separation between the different cavitating regions and, if they are sufficiently close, they are considered as an unique cavitating region. Otherwise, if the cavitating regions are sufficiently distant, they are considered as effectively separated and only the length of the first one is taken into account.

D. Fourier analysis of the cavity length

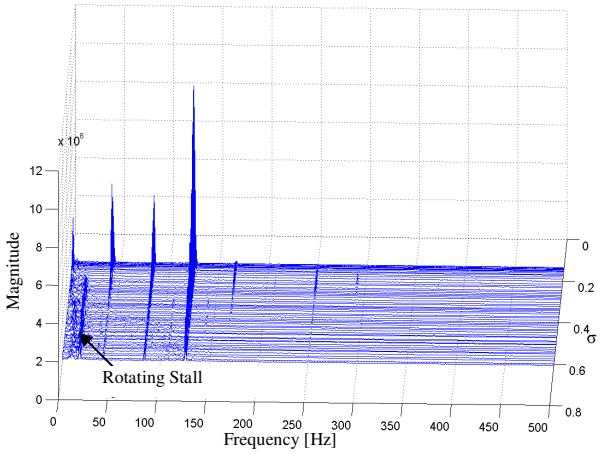

Figure 15. Waterfall plot of the power spectrum of the inlet pressure fluctuations in the FIP inducer at Φ=0.034, Ω=2500 rpm [Cervone *et al.*[3]]

The plots in Figure 14 refer to flow conditions at which rotating stall instability has been detected by means of cross-correlation and phase analysis of the pressure oscillations (Figure 15).

Figure 14 shows an example of oscillating cavity length. In order to understand the nature of these oscillations, Fourier analysis of the non-dimensional tip cavity length has been carried out.

As shown in Figure 16, a well defined peak is detected in the power spectrum at a frequency of 15.7 Hz (f_1). The detected rotating stall[3] had a frequency of about 0.34Ω in a fixed coordinate frame (8.5 Hz at 1500 rpm). In a coordinate frame rotating with the blades (as the one used to estimate the cavity length) this frequency becomes 16.5 Hz, very close to the value of

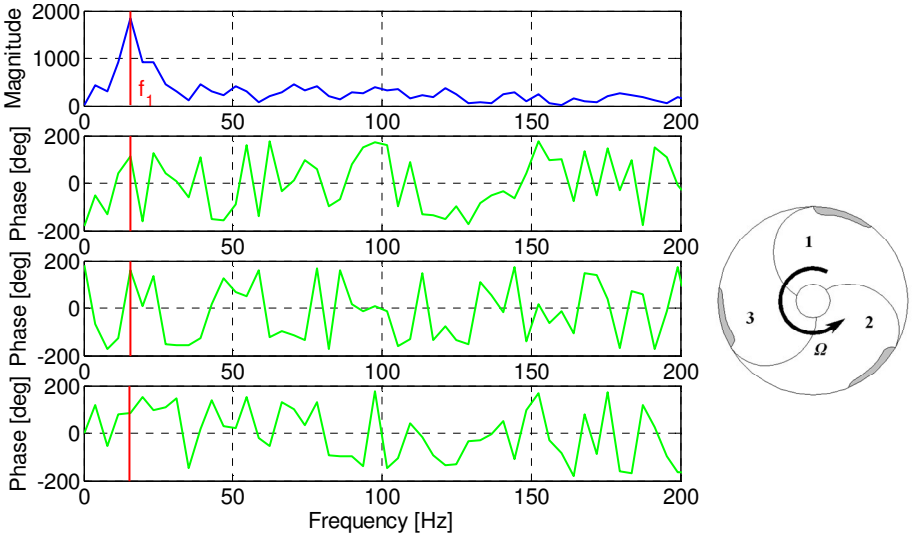

Figure 16. Power spectrum of the tip cavity length on third blade (blue). Phase of the cross-correlation between 3rd and 2nd blade (second plot), 2nd and 1st blade (third plot), 1st and 3rd blade (fourth plot).

f_1. Figure 16 shows that the cross-correlation phases are 116° (blade 3-blade 2), 160° (blade 2-blade 1) and 87° (blade 1-blade 3). This means that the phenomenon is rotating clockwise in the rotating coordinate frame. The ratio of the mean angular separation of two adjacent cavitating regions to the relative cross-correlation phase is about one and this means that the oscillation involves just one single rotating cell. From these results, it is clear that the instability denoted by f_1 has characteristics similar to the rotating stall previously detected on the same inducer.

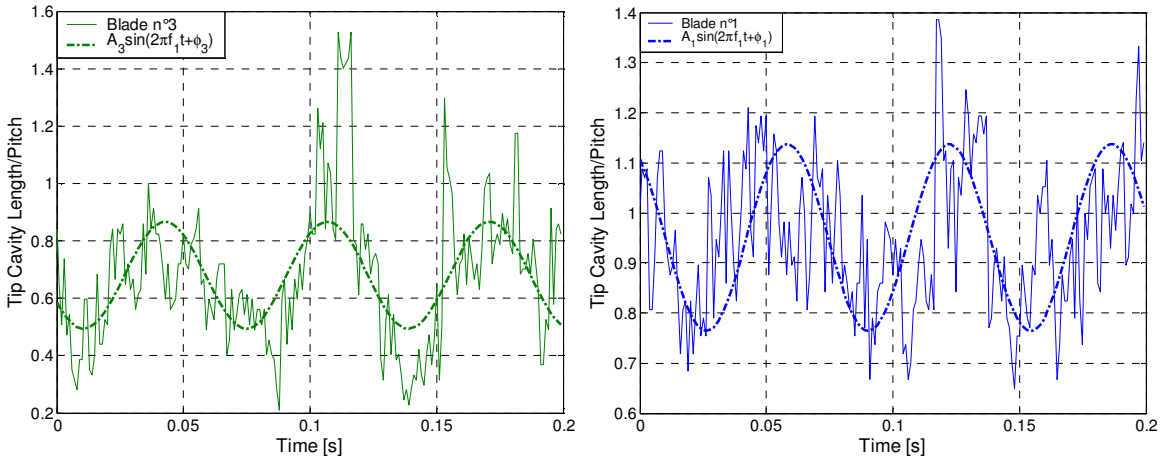

(a) **(b)**

Figure 17. Sinusoidal signal at frequency f_1 superimposed to the measured non-dimensional tip cavity length for blade 3 (a) and blade 1 (b).

Figure 17(a) shows a sinusoidal signal at frequency f_1, whose magnitude and phase have been calculated using a trial-and-error technique, superimposed to the non-dimensional tip cavity length on the third blade, while Figure 17(b) shows the same sinusoidal signal shifted of an angle equal to the phase of the cross-correlation between blade 3 and blade 1. Figure 18(a) shows the sinusoidal signals of Figure 17 together with that obtained for the remaining blade (same frequency, phase calculated from the cross-correlation analysis): the cavity propagates clockwise from the first blade to the third blade. It is also evident that the mean cavity length on the third blade is lower than the other two (asymmetric cavitation, Figure 18 (b)).

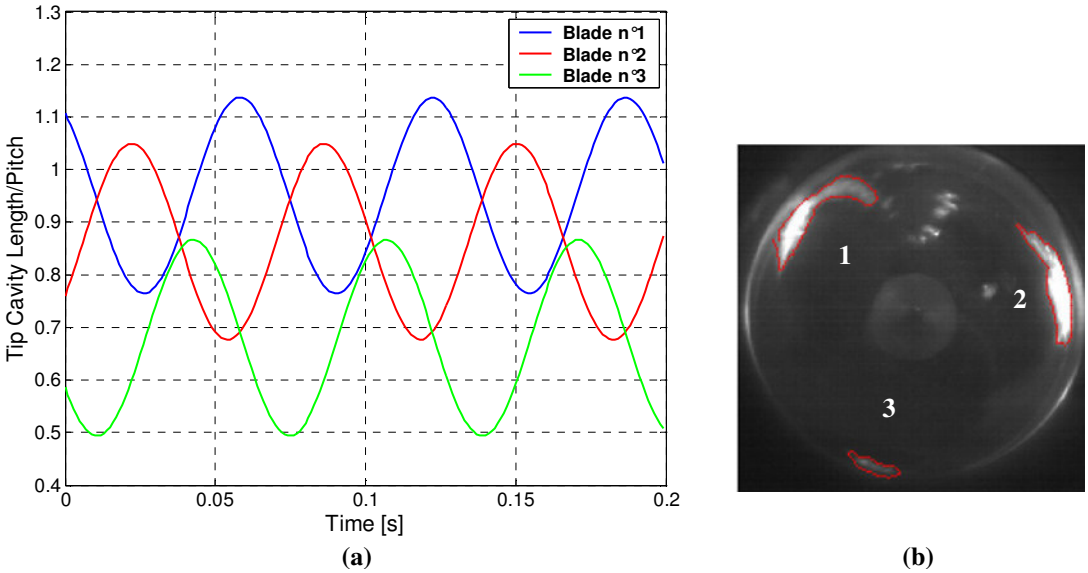

(a) **(b)**

Figure 18. Oscillation of the cavity length on the blades of the FIP inducer (a). Example of asymmetric blade cavitation (b).

VI. Conclusions

The research activity has allowed for the development and successful validation of a viable and effective tool, based on optical processing of high-speed video movies for quantitative analysis and diagnostics of cavitation instabilities in turbopump inducers. The capabilities of the semi-automatic algorithm created to implement the proposed technique have been improved by developing a procedure for the estimation of the frontal cavitating surface and the extension of the cavitating regions on the blades.

Preliminary application of the above technique to the analysis of cavitation in a test inducer lead to the detection of the same rotating stall instability previously observed under the same operating conditions by means of Fourier analysis of the inlet pressure signals. The results confirm the potential of the proposed method in the characterization of cavitation-induced instabilities and suggest the possibility of extracting additional useful information on the nature, extent and location of the cavitating regions on the inducer blades by means of more spatially-resolved processing of the video images.

Acknowledgments

The present activity has been funded by the Agenzia Spaziale Italiana under contract No. I/016/05/0 for fundamental research, whose support is gratefully acknowledged. The authors would like to express their gratitude to Profs. Mariano Andrenucci, Renzo Lazzeretti and Fabrizio Paganucci of the Dipartimento di Ingegneria Aerospaziale, Università di Pisa, Pisa, Italy, for their constant and friendly encouragement.

References

[1]Stripling L.B. and Acosta A.J., 1962, "Cavitation in Turbopumps – Part 1", ASME J. Basic Eng., Vol. 84, pp. 326-338.

[2]Brennen C.E., 1994, "Hydrodynamics of Pumps", Concepts ETI, Inc. and Oxford University Press.

[3]Cervone A., Testa R., Bramanti C., Rapposeli E. and d'Agostino L., 2005, "Thermal Effects on Cavitation Instabilities in Helical Inducers", AIAA Journal of Propulsion and Power, Vol. 21, No. 5, Sep-Oct 2005, pp. 893-899.

[4]Cervone A., Torre L., Bramanti C., Rapposelli E. and d'Agostino L., 2005, "Experimental Characterization of the Cavitation Instabilities on the Avio FAST2 Inducer", 41th AIAA/ASME/SAE/ASEE Joint Propulsion Conference, Tucson, Arizona, USA.

[5]Tsujimoto Y., Yoshida Y., Maekawa Y., Watanabe S., Hashimoto T., 1997, "Observation of Oscillating Cavitation of an Inducers", ASME J. Fluids Eng. ing, Vol. 119, pp. 775-781.

[6]Hashimoto T., Yoshida M., Watanabe M., Kamijo K., Tsujimoto Y., 1997, "Experimental Study of Rotating Cavitation of Rocket Propellant Pump Inducers", J. Propulsion and Power, Vol. 13, N. 4., pp. 488-494.

[7]K. Kamijo, T. Shimura, Y. Tsujimoto, “Exprimental and Analytical Study of Rotating Cavitation”, Cavitation and gas liquid flow in fluid machinery and devices, ASME 1994.

[8]Rapposelli E., Cervone A. & d’Agostino L., 2002, “A New Cavitating Pump Rotordynamic Test Facility”, AIAA Paper 2002-4285, 38th AIAA/ASME/SAE/ASEE Joint Propulsion Conference, Indianapolis, IN, USA, July 8-11.

[9]Gonzalez R.C., Woods R.E., 2002, “Digital Image Processing”, Prentice-Hall.

[10]Hiscock J.E., Mouland D., Wang G. and Ching C.Y., 2000, “Gas Bubble Velocity Measurements Using High-Speed Images of Gas-Liquid Flows”, ASME FEDSM summer meeting, Boston, Massachusetts, USA, 2000.

[11]Kato K., Matudaira Y. and Obara H., 2003, “Flow Visualization of Cavitation with Particle and Bubble Image Processing”, ASME FEDSM summer meeting, Honolulu, Hawaii, USA, 2003.

[12]Otsu N., “A Threshold Selection Method from Gray-Level Histograms”, IEEE Transactions on Systems, Man and Cybernetics, vol. 9, no. 1, pp. 62-66, 1979.